

Magnetic-field-tunable anisotropic black-body radiation in dynamical axion insulators

E. Kochems,¹ G. Quintero Angulo,^{1,2} R. Egger,¹ C. Müller,¹ and S. Villalba-Chávez^{1,*}

¹*Institut für Theoretische Physik, Heinrich-Heine-Universität Düsseldorf,
Universitätsstr. 1, 40225 Düsseldorf, Germany*

²*Departamento de Física Teórica, Facultad de Física, Universidad de la Habana,
San Lázaro y L, Vedado, La Habana 10400, Cuba*

(Dated: July 25, 2024)

An antiferromagnetic order breaking simultaneously the time-reversal and space-inversion symmetries in topological insulators might give rise to dynamical axion-like fields in the form of longitudinal spin waves. The consequences of the associated axion-polariton state on the thermal radiation are investigated. Planck's radiation law is shown to exhibit remarkable anisotropic behavior as a result of the strong refraction caused by the heat-matter interaction. A crossover scenario at low temperature is identified and an associated regime in which the system's internal energy does not scale with the traditional fourth power of the temperature is revealed. We show that the polarization purity of the heat radiation and its angular distribution can be controlled via the magnetic field, paving the way toward a directional-tunable mechanism for thermal quanta manipulation and storage.

Introduction—Solving the strong CP problem through the Peccei-Quinn mechanism led to the emergence of the QCD axion [1–3] and has since been a paradigm for the broader class of axions occurring in various Standard Model extensions [4–12], some of which put them forward as viable candidates for nonbaryonic dark matter [13–17]. While the original QCD-axion was ruled out shortly after its prediction [18, 19], experimental endeavors toward the detections of axion-like particles are nowadays being carried out worldwide [20, 21], based predominantly on the axion-diphoton coupling that characterizes the theoretical framework of axion-electrodynamics (AED) [22]. Despite compelling theoretical arguments supporting their existence, no axion has been detected to date, thus suggesting a feeble interplay between these elusive particles and the well-established Standard Model constituents.

With the plausible realization of dynamical axion-like fields in topological insulators with broken spatial inversion and time-reversal symmetries, an enticing landscape toward the comprehension of axion physics has been opened [23]. Indeed, dynamical axion insulators (DAIs), such as the already synthesized MnBi₂Te₄ flakes [24–27], constitute suitable platforms for proof-of-principle tests of various phenomena on which axion searches rely. Moreover the intrinsic characteristics of the medium, such as stiffness and topology, along with the knowledge of the associated axion quasiparticle mass, make DAIs ideal for investigating phenomenology beyond the justifiable perturbative regime that the counterpart of particle physics extensively utilizes. Theoretical studies in this direction have revealed a few emerging phenomena closely linked to the hallmark medium's magnetoelectric response [28–32], and in line, DAI-based methods to detect dark-matter axions have been proposed [33, 34]. Moreover, recent arguments support the idea that the realization of cavity-based axion-polaritons [35] could ben-

efit the quantum control of light-matter interaction over other widely studied systems, like the qubit in superconducting circuits and the mechanical oscillator in cavity optomechanics [36, 37].

The primary reasons for these prospects stem from DAI's seemingly favorable cooling feature and the opportunity to further control the interaction strength through an external magnetic field [38]. However, high field strengths could induce significant changes in the axion quasiparticle mass and thus modify the critical temperature for condensation of the massive branch of the axion-polariton ensemble, making it difficult to cool to the ground state even if it is characterized by a low population. In this context, the question arises whether additional consequences associated with the explicit breakdown of spatial isotropy may also result in nontrivial effects that significantly influence the system's thermodynamic control. Indeed, in this letter we show that, near the critical boundary between the antiferromagnetic and paramagnetic phases, the intrinsic refraction of the axion-polariton state renders Planck's radiation law exhibit a field-tunable anisotropy. This remarkable feature enables the control of directional-dependent macroscopic properties of thermal radiation under equilibrium conditions. Our research focuses on a scenario where the magnetic field competes with temperature to dominate the phenomenological picture. We thereby reveal qualitatively new properties of DAIs that are unaffected by the topological state of the insulator and discuss potential applications.

Thermal Field Theory Approach—Let us consider a DAI sample characterized by a volume $V = L_x L_y L_z$. We describe the equilibrium black-body radiation inside the insulator using AED. By adopting rationalized Gaussian units with $c = \hbar = k_B = \epsilon_0 = 1$, this theoretical frame-

*Electronic address: villalba@uni-duesseldorf.de

work is characterized by the action [23]

$$\Gamma = \int d^4x \left\{ 4\pi Jg^2 \left[(\partial_t \delta\theta)^2 - (v_i \partial_i \delta\theta)^2 - m^2 \delta\theta^2 \right] + \frac{1}{2} (\mathbf{D} \cdot \mathbf{E} - \mathbf{H} \cdot \mathbf{B}) + \frac{\alpha}{\pi} (\bar{\theta} + \delta\theta) \mathbf{E} \cdot \mathbf{B} \right\}. \quad (1)$$

Here, $\mathbf{D} = \epsilon \mathbf{E}$ and $\mathbf{H} = \mu^{-1} \mathbf{B}$ are the electric and magnetic displacement vectors, with ϵ and μ denoting the respective dielectric constant and magnetic permeability, with material stiffness J , constant g , and $\alpha = e^2/(4\pi)$ referring to the fine structure constant. We note that, the static axion field $\bar{\theta}$ takes $\bar{\theta} = \pi$ in time-reversal invariant topological insulators, whereas $\bar{\theta} = 0$ in topologically trivial insulators [32]. In Eq. (1), $v_{i=x,y,z}$ stands for the group velocity components of the “free” low-energy spin-wave $\delta\theta$ with $|\delta\theta| < \bar{\theta}$, whereas m refers to its mass. This fluctuating field corresponds to the projection of the spontaneous antiferromagnetic order parameter—Néel’s field—onto the easy-axis of the magnetic topological insulator. In the following, we shall employ a rescaled version of $\delta\theta$: $\sqrt{8\pi Jg^2}\delta\theta \rightarrow \phi$, which results in a multiplicative renormalization of the gauge coupling $\alpha \rightarrow \alpha/\sqrt{8\pi Jg^2}$.

Heat radiation will be identified with small-amplitude electromagnetic waves $a_\mu(t, \mathbf{x})$ describing the linear response of the system to the presence of a constant magnetic background \mathbf{B} . As a consequence, we will focus on the action that results from Eq. (1) when the electromagnetic fields \mathbf{E} and \mathbf{B} are substituted by $\mathbf{e} = -\nabla a_0 - \partial \mathbf{a}/\partial t$ and $\mathbf{B} + \mathbf{b}$ with $\mathbf{b} = \nabla \times \mathbf{a}$, respectively, and only nontrivial bilinear combinations in $a_\mu(t, \mathbf{x})$ are retained:

$$S = \int d^4x \left\{ -\frac{\mathbf{B}^2}{2\mu} + \frac{1}{2} [e^2 - c'^2 \mathbf{b}^2] + \kappa \phi \mathbf{e} \cdot \mathbf{B} + \frac{1}{2} [(\partial_t \phi)^2 - (v_i \partial_i \phi)^2 - m^2 \phi^2] \right\}, \quad (2)$$

where the rescaling $a_\mu(t, \mathbf{x}) \rightarrow a_\mu(t, \mathbf{x})/\sqrt{\epsilon}$ has been carried out afterwards. In the action above, $c' = (\epsilon\mu)^{-1/2}$ is the speed of light in the medium, whereas $\kappa = \alpha/\sqrt{(2\pi)^3 J g^2 \epsilon}$ characterizes the coupling strength of the mixing between $\phi(t, \mathbf{x})$ and $a_\mu(t, \mathbf{x})$ mediated by \mathbf{B} .

Establishing the corresponding Helmholtz free energy $\mathcal{F} = -\beta^{-1} \ln \mathcal{Z}$ requires adopting the imaginary time formalism $t \rightarrow -i\tau$ with $0 \leq \tau \leq \beta$ and $\beta = T^{-1}$ denoting the inverse temperature. In this context, the boson fields $\phi(x)$ and $a_\mu(x)$ with $x_\mu = (\mathbf{x}, \tau)$ and $\mu = 1, 2, 3, 4$, are promoted to periodic functions in the variable τ . The calculation of the required partition function can be carried out by extending the covariant Fadeev-Popov ansatz [39, 40] to the case under consideration: $\int \mathcal{D}\chi \delta(\mathcal{G}[{}^\chi a_\mu]) \det [\delta\mathcal{G}[{}^\chi a_\mu]/\delta\chi]_{\chi=0} = 1$. Here, the gauge-transformed field is ${}^\chi a_\mu = a_\mu + \partial_\mu \chi$. The expression above combines the gauge-fixing function $\mathcal{G}[a_\mu] = -c'^2 \nabla \cdot \mathbf{a} - \partial_\tau a_4 + s$ with $s(x)$ denoting an arbitrary spacetime depending scalar. Moreover, $\det [\delta\mathcal{G}[{}^\chi a_\mu]/\delta\chi]_{\chi=0} = \det(-\square_{x, \tilde{x}})$ is the Fadeev-Popov determinant with $\square_{x, \tilde{x}} \equiv \partial_x^2 \delta^4(x - \tilde{x})$ and $\partial^2 = c'^2 \nabla^2 + \partial_\tau^2$.

As such, the partition function is independent of the function $s(x)$. Upon weighting it with the Gaussian factor $\exp \left[-\frac{1}{2\zeta c'^2} \int_X d^4x s^2 \right]$ with $\int_X d^4x \equiv \int_0^\beta d\tau \int_V d^3x$ and a gauge-fixing parameter ζ , and integrating functionally over $s(x)$, the gauge-fixing term rises to the exponent, enabling us to express $\mathcal{Z} = \exp \left[-\frac{\beta V}{2\mu} B^2 \right] \mathcal{Z}_{\text{AED}}$ with

$$\mathcal{Z}_{\text{AED}} = \det(-\square_{x, \tilde{x}}) \int_{\text{Periodic}} \mathcal{D}a \mathcal{D}\phi e^{-S_E}. \quad (3)$$

Here, S_E is the Euclidean action resulting from Eq. (1) combined with the gauge-fixing term in the Feynman gauge [$\zeta = 1$]. Explicitly,

$$S_E = \int_X d^4x \left\{ -\frac{1}{2} a_\alpha \partial^2 \delta_{\alpha\beta} a_\beta + \frac{1}{2} \phi [-\partial_v^2 + m^2] \phi + j\phi \right\},$$

where integrations by parts have been carried out. Here, $\partial_v^2 = \partial_\tau^2 + (v_i \partial_i)^2$, and $\delta_{\alpha\beta} = \text{diag}(1, 1, 1, 1/c'^2)$. In S_E , $j(x) = \frac{i}{2} \kappa \tilde{F}_{\alpha\beta} f_{\alpha\beta}$ is a background-dependent source for the axion field with $f_{\alpha\beta} = \partial_\alpha a_\beta - \partial_\beta a_\alpha$, $\tilde{F}_{\alpha\beta} = \frac{1}{2} \epsilon_{\alpha\beta\mu\nu} F_{\mu\nu}$, $\epsilon_{1234} = 1$. In this context, $F_{\alpha\beta}$ is the external electromagnetic tensor with components $F_{j4} = 0$ and $F_{j\ell} = -\epsilon_{j\ell k} B_k$ and $j, \ell = 1, 2, 3$. We remark that S_E does not depend on the static axion field $\bar{\theta}$, which implies that the partition function is not influenced by the topology of the insulator.

The functional integrations in Eq. (3) can be straightforwardly calculated owing to the integrand’s Gaussian nature. This feature guarantees, indeed, that the contribution of small amplitude waves dominates over the remaining ones. Upon carrying out the one over $\phi(x)$,

$$\mathcal{Z}_{\text{AED}} \propto \det(-\square_{x, \tilde{x}}) [\det(-\square_{x, \tilde{x}}^v + m_{x, \tilde{x}}^2)]^{-\frac{1}{2}} \times \int \mathcal{D}a e^{-\int_X d^4x \int_X d^4\tilde{x} [-\frac{1}{2} a_\alpha(x) D_{\alpha\beta}^{-1}(x, \tilde{x}) a_\beta(\tilde{x})]}. \quad (4)$$

Here, $D_{\alpha\beta}^{-1}(x, \tilde{x}) = -\square_{x, \tilde{x}} \delta_{\alpha\beta} + \Pi_{\alpha\beta}(x, \tilde{x})$ denotes the inverse photon propagator that involves the polarization tensor $\Pi_{\alpha\beta}(x, \tilde{x}) = -\kappa^2 \tilde{F}_{\alpha\sigma} [\partial_\sigma^x \partial_\mu^{\tilde{x}} \Delta_E(x, \tilde{x})] \tilde{F}_{\mu\beta}$ —see Fig. 1a—mediated by the Euclidean axion propagator $\Delta_E(x, \tilde{x})$ [41, 42]. In Eq. (4) we have used the shorthand notation $\square_{x, \tilde{x}}^v \equiv \partial_v^2 \delta^4(x - \tilde{x})$ and $m_{x, \tilde{x}}^2 \equiv m^2 \delta^4(x - \tilde{x})$. Next, we express $a_\alpha(x)$ as a Fourier series and carry out the integration. As a consequence,

$$\mathcal{Z}_{\text{AED}} = \prod_{\mathbf{n}, \mathbf{q}} [\beta^2 (\omega_n^2 + \omega_o^2)] [\beta^2 (\omega_n^2 + v_i^2 q_i^2 + m^2)]^{-\frac{1}{2}} \times [\beta^8 \det(\delta_{\alpha\beta}(\omega_n^2 + \omega_o^2) + \Pi_{\alpha\beta}(-q))]^{-\frac{1}{2}}, \quad (5)$$

where $\omega_o = c' |\mathbf{q}|$ is the ordinary photon dispersion law in the medium and $\omega_n = 2n\pi/\beta$ are the bosonic Matsubara frequencies. In Eq. (5) an unessential proportionality factor has been ignored, $\Pi_{\alpha\beta}(q) = \kappa^2 \Delta_E(q) \tilde{F}_{\alpha\lambda} q_\lambda \tilde{F}_{\beta\sigma} q_\sigma$ with $\Delta_E(q) = (\omega_n^2 + v_i^2 q_i^2 + m^2)^{-1}$ and $q_\mu = (\mathbf{q}, \omega_n)$.

Next, we substitute Eq. (5) into Eq. (3). The resulting expression for \mathcal{Z} is inserted into the Helmholtz free

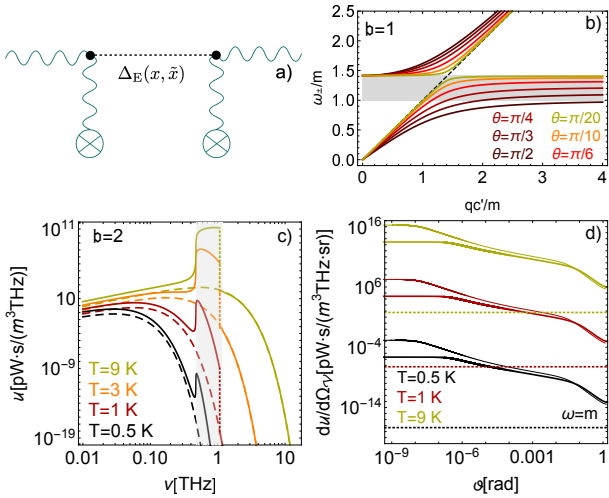


FIG. 1: a) Feynman diagram of the polarization tensor driven by a magnetic field [wavy lines ending with crossed blobs] and mediated by a quantum fluctuation of the spin-wave field. b) Dispersion relations. The diagonal dashed line is linked to the ordinary photon mode (ω_o), whereas the gray band shows the maximum gap. While the lower (massless) branch is associated with extraordinary photons (ω_-), the upper (massive) one is linked to axions (ω_+). Here, $\theta \in [0, \pi]$ is the angle between the wave vector $\mathbf{n} = \mathbf{q}/|\mathbf{q}|$ and \mathbf{B} . c) Black-body radiation spectrum. Here, the gray band shows the maximum frequency gap exhibited between ω_- and ω_+ at $b = 2$. While the dashed curves display the spectrum of the ordinary mode, those in thick style that end on the right of the gap are linked to the extraordinary mode. The thick curves following the discontinuities at the right of the gap describe the axion like spectrum. d) Angular distribution of the internal energy density due to extraordinary photons at $\omega = m$. Here, the solid angle is $d\Omega_v \equiv d\varphi d\cos(\vartheta)$. Curves sharing a color are linked to a common temperature at $b = 1$ (thick) and $b = 5$ (thin). The contributions resulting from the ordinary mode are depicted by dotted lines.

energy's defining expression. After carrying out the sum over the Matsubara frequencies we find $\mathcal{F} = \frac{V}{2\mu} B^2 + \mathcal{F}_{\text{vac}} + \mathcal{F}_{\text{st}}$ with $\mathcal{F}_{\text{vac}} = \frac{1}{2} V \sum_i \int_{\Lambda} \frac{d^3 q}{(2\pi)^3} \omega_i$ the vacuum contribution and $\mathcal{F}_{\text{st}} = \frac{V}{\beta} \sum_i \int_{\Lambda} \frac{d^3 q}{(2\pi)^3} \ln(1 - e^{-\beta\omega_i})$ the statistical one. Here, we have gone over to the continuum limit $V \rightarrow \infty$, bounding the integration domain to a region Λ with $\Lambda^{1/3} \sim \mathcal{O}(0.1)$ eV where the low energy description Eq. (1) applies. In \mathcal{F}_{vac} and \mathcal{F}_{st} , the Latin index i runs over $i = o, \pm$, covering the massless—photon-like excitations—and massive branches of the polariton state, which are linked with the extraordinary (ω_-) and axion-like (ω_+) dispersion relations $\omega_{\mp}^2 = \frac{1}{2}(\omega_o^2 + w_*^2) \mp \frac{1}{2}\sqrt{(\omega_o^2 - w_*^2)^2 + 4m^2 b^2 c'^2 q_\perp^2}$, respectively. Here, q_\perp is the momentum in the plane perpendicular to \mathbf{B} . The previous relations depend on the ordinary photon dispersion law ω_o and $w_* = [v_i^2 q_i^2 + m_*^2]^{1/2}$, where $m_* = m(1 + b^2)^{1/2}$ is the dressed axion mass with $b = B/B_{\text{crit}}$ and $B_{\text{crit}} = m/\kappa$ denoting the characteristic magnetic field scale of AED. Here, κ is the axion-photon

coupling in Eq. (2).

Results and Discussion—In the following, we carry out a numerical evaluation, taking the benchmark parameters estimated for the antiferromagnetic phase of $(\text{Bi}_{1-x}\text{Fe}_x)_2\text{Se}_3$ with a nominal doping concentration $\approx 3.5\%$ [23, 43]. In this case, the factor $Jg^2 \approx 450$ eV² and the dynamical axion mass can reach values as small as $m \approx 2$ meV near the critical boundary between the antiferromagnetic and paramagnetic phases. The values of these parameters are generally temperature-dependent [44, 45], lifting the typical mass of the axion-like quasiparticle to $m \sim \mathcal{O}(1)$ eV far from the phase boundary [45, 46]. Conversely, in the vicinity of the critical limit, the mass changes with the doping concentration but varies very slowly with temperature, enabling us to treat the benchmark mass as a constant [44]. Moreover, the estimated dielectric constants in this material are $\epsilon \approx 25$ and $\mu \sim 1$, leading to a speed of light $c' \approx 0.2$ and a characteristic magnetic field scale $B_{\text{crit}} \approx 2.35$ T that can be easily overpassed. Hereafter, we will consider the velocity components of a “free” axion to be equal and of the order of the spin wave speed, which we take $v_{x,y,z} = v_s = 10^{-4}$ [34, 47, 48]. Fig. 1b shows the mutual repelling behavior of the resulting dispersion relations that characterizes the axion-polariton state.

Since we are interested in assessing how the previously described field-dependent dispersion phenomenon affects the medium's thermal properties, the black body spectra will be our first focus of interest. To this end, we primarily investigate the internal energy density $\mathcal{U} = \frac{1}{V} \frac{\partial(\beta\mathcal{F})}{\partial\beta} = \sum_i \mathcal{U}_i$. Indeed, by going over to spherical variables and neglecting the vacuum contribution,

$$u_i = \frac{d\mathcal{U}_i}{d\nu} = \frac{4\pi^2}{c'^2} \frac{\nu^3}{e^{2\pi\nu} - 1} \int_0^\pi d\theta \frac{n_i^2}{n_o^2} \frac{\sin\theta}{|\mathbf{v}_i \cdot \mathbf{n}|}. \quad (6)$$

Here, $n_i = |\mathbf{q}|/\omega_i$ and $\mathbf{v}_i = \nabla_{\mathbf{q}}\omega_i$ stand for mode- i 's refraction index and group velocity, respectively. The formula above constitutes our main analytic result. Here, the factor $|\mathbf{v}_i \cdot \mathbf{n}|^{-1}$ is the Jacobian resulting from adopting $\nu = \omega/(2\pi)$ as integration variable. The expression above shares certain similarities with Planck's radiation law for dispersive anisotropic media [49, 50]. Fig. 1c summarizes the behavior of u_i in a DAI when $b = 2$. The shown frequency range covers quasiparticle energies $\omega < 42$ meV below the material's bulk gap $\sim \mathcal{O}(0.1)$ eV as required by the low-energy description. Moreover, the sample extension $L_{x,y,z} \sim \mathcal{O}(1)$ cm limits $|q_{x,y,z}| \gg \mathcal{O}(10)$ μeV , providing the lowest frequency bound $\nu \gg \mathcal{O}(10^{-1})$ GHz, corresponding to $\omega \gg \mathcal{O}(1)$ μeV , from which the results are expected to be reliable. As one could anticipate, the extraordinary spectrum shows a discontinuity at $\nu = m_*/(2\pi)$. The remarkable departure that the extraordinary thermal spectrum undergoes from the ordinary one is rooted in the flattening that its dispersion relation exhibits (see Fig. 1b). This information is encoded in Eq. (6) within the field-dependent factor $n_-^2/|\mathbf{v}_- \cdot \mathbf{n}|$. We point out that such a property implies that extraordinary quanta with

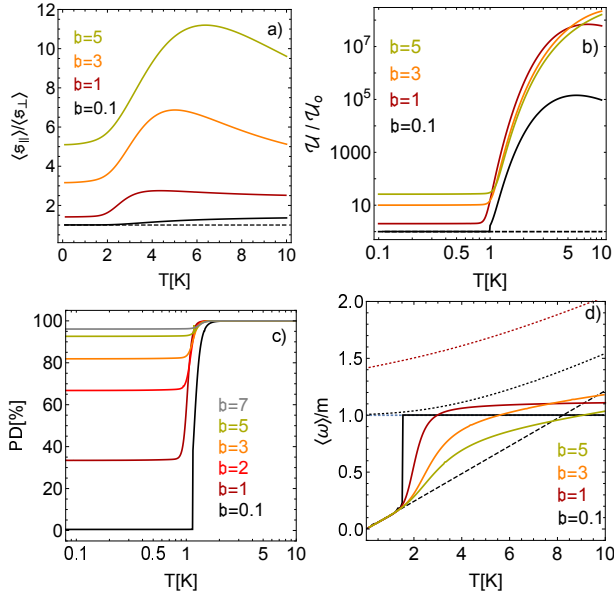


FIG. 2: a) Ratio of the positive energy flux parallel to and perpendicular to \mathbf{B} as a function of temperature for different field strength parameters b . The dashed line is associated with the ordinary modes, while thick curves are linked to the extraordinary photons. b) Dependence of internal energy density \mathcal{U} on the system’s temperature for different magnetic fields. The dashed line gives for comparison a ratio of unity. c) Polarization degree (PD) of heat radiation in DAI vs temperature for different b . d) Mean energy of extraordinary photons (solid) and axion-like modes (dotted) vs temperature. Curves sharing color correspond to a common magnetic field parameter. The results of the massive mode corresponding to $b = 3$ and $b = 5$ lie outside the shown range. The black dashed line displays Wien’s displacement law of the ordinary spectrum, i.e., $\omega_o^{\max} = \tilde{\kappa}T$ with $\tilde{\kappa} = 2.431 \times 10^{-1}$ meV/K.

$q_{\perp} > m/c'$ are characterized by a perpendicular group velocity component $v_{\perp,-} = |\partial\omega_-/\partial q_{\perp}| \ll c'$.

Except for ordinary photons, the direction of energy transfer of the extraordinary and axion-like modes differs from their respective wave vectors. If $\vartheta = \tan^{-1}(v_{\perp,-}/v_{\parallel,-})$ and $\theta = \tan^{-1}(q_{\perp}/q_{\parallel})$ are the respective group and phase velocity angles relative to the external field with $v_{\parallel,-} = \partial\omega_-/\partial q_{\parallel}$, then $\tan(\vartheta) = \tan(\theta)\partial q_{\parallel}^2/\partial q_{\perp}^2$, where q_{\parallel} must be understood here as a function of q_{\perp} keeping the energy ω_- constant. This connection enables us to parametrically generate a graph exhibiting how the energy density due to extraordinary photons varies with the angle ϑ (solid curves in Fig. 1d). Observe that the thick curves tend to be peaked at $\vartheta \approx 0$, and that, the stronger the field, the more prominent this behavior is. The results point out that, even though the states of extraordinary quanta might be characterized by a non-zero q_{\perp} with $m/c' < q_{\perp} < \mathcal{O}(0.1)$ eV, the “energy transport” is more likely to occur parallel to \mathbf{B} .

To further confirm this statement, we have analyzed the ratio between the positive energy fluxes parallel and perpendicular to \mathbf{B} linked to the extraordinary mode.

These quantities follow from the Cartesian components of the Poynting vector $\langle \mathbf{s}_- \rangle = V \int_{\Lambda} \frac{d^3 q}{(2\pi)^3} \frac{\omega_-}{\exp(\beta\omega_-)-1} \mathbf{v}_-$ averaged over the part of the ensemble whose group velocity components are positive [51]. The behavior of the ratio $\langle s_{\parallel} \rangle / \langle s_{\perp} \rangle$ with temperature is shown in Fig. 2a for magnetic field strengths that fall into the range of values permitted in the nontrivial topological phase [35]. Since $\langle s_{\parallel} \rangle / \langle s_{\perp} \rangle > 1$ with $s_{\perp} \equiv s_x = s_y$, it is then evident that the heat radiation is distributed anisotropically, and that extraordinary thermal modes propagating parallel to \mathbf{B} exceed those propagating transversal to it. Manifestly, Fig. 2a shows that this property is more pronounced as B increases. Indeed, for $T \approx 6$ K and $b = 5$, $\langle s_{\parallel} \rangle$ is an order of magnitude larger than $\langle s_{\perp} \rangle$. Observe that, by comparing the values of different curves at a given temperature a highly nonlinear dependence on the magnetic field is revealed. Unlike the previous case, the “energy transport” of the axion-like mode along \mathbf{B} diminishes monotonically with both temperature and magnetic field rising. This behavior is, however, not shown in Fig. 2a.

Noteworthy, as the area below the extraordinary spectrum (see Fig. 1c) increases by raising the temperature its contribution to the energy density outweighs those associated with the remaining propagation modes. Fig. 2b exhibits the temperature dependence of the total energy density in units of $\mathcal{U}_o = \frac{8\pi^2}{c^3} \int_{\nu_{\min}}^{\infty} \frac{d\nu \nu^3}{\exp(2\nu/T)-1}$. To meet the limitations outlined below Eq. (6), the lowest integration limit here and in the contribution linked to the extraordinary mode was taken $\nu_{\min} = 10$ GHz. The findings exhibited suggest that a crossover occurs at $T_* \approx 1.5$ K between regions with different phenomenologies. Indeed, for $T < T_*$, the internal energy density of the axion-polariton ensemble $\mathcal{U}_- + \mathcal{U}_+ \approx \mathcal{U}_- \approx \mathcal{C}\mathcal{U}_o$ where \mathcal{C} is a B -dependent constant. This is because, at lower temperatures, the area below the extraordinary spectrum (see Fig. 1c) is still dominated by a Planck profile, although dressed by the field-dependent factor $n_-^2/|\mathbf{v}_- \cdot \mathbf{n}|$. The temperature scaling of \mathcal{U}_- is, however, significantly stronger than $\mathcal{U}_o \approx \pi^2 T^4/(30c^3)$ for $T > T_*$, outweighing the contribution of the ordinary photon gas by five orders of magnitude at $T \approx 5.7$ K when $b = 1$. The fact that, in the exposed temperature range, $\mathcal{U}_- > \mathcal{U}_o$ is an indication that the number of extraordinary photons exceeds the ordinary ones, and the heat radiation tends to polarize. Fig. 2c is meant to support this statement. It depicts that, at $T < T_*$, the polarization degree $PD = (N_- - N_o)/(N_- + N_o)$ with $N_i = V \int_{\Lambda} \frac{d^3 q}{(2\pi)^3} \frac{1}{\exp(\beta\omega_i)-1}$ can be controlled efficiently through the magnetic field strength. Moreover, it reveals that, regardless of B , the thermal radiation in a DAI acquires a high polarization purity $\approx 100\%$ when $T_* < T < 10$ K. Finally, in Fig. 2d, the solid curves display the behavior of the mean energy $\langle \omega_i \rangle$ of the involved quasiparticles as the temperature varies for different magnetic field strengths. These outcomes reveal that, in contrast to Wien’s displacement law of the ordinary photon spectrum (dashed line), $\langle \omega_{\pm} \rangle$ depend nonlinearly on T .

Conclusions—The thermal radiation properties in DAIs are determined by the strong birefringence that the inherent axion-polariton state transfers to the statistical ensemble. Magnetic field and temperature are suitable parameters for quantum controlling the distribution, strength, and polarization of heat radiation in DAIs. The reported black-body radiation law in DAI materials applies to both topological and trivial phases. Our findings offer prospects toward an out-of-contact, directionally-tunable mechanism for manipulating heat radiation in

DAIs.

Acknowledgments—GQA gratefully acknowledges the support of the Alexander von Humboldt Foundation. RE acknowledges funding by the Deutsche Forschungsgemeinschaft (DFG, German Research Foundation), under Projektnummer 277101999 – TRR 183 (project C01), and under Germany’s Excellence Strategy – Cluster of Excellence Matter and Light for Quantum Computing (ML4Q) EXC 2004/1 – 390534769.

-
- [1] R. D. Peccei and H. R. Quinn, CP Conservation in the Presence of Pseudoparticles, *Phys. Rev. Lett.* **38**, 1440 (1977).
- [2] F. Wilczek, Problem of Strong p and t Invariance in the Presence of Instantons, *Phys. Rev. Lett.* **40**, 279 (1978).
- [3] S. Weinberg, A New Light Boson?, *Phys. Rev. Lett.* **40**, 223 (1978).
- [4] M. Dine, W. Fischler and M. Srednicki, A simple solution to the strong CP problem with a harmless axion, *Phys. Lett. B* **104**, 199 (1981).
- [5] A. R. Zhitnitskii, On Possible Suppression of the Axion Hadron Interactions, *Yad. Fiz.* **31**, 497 (1980); [Sov. J. Nucl. Phys. **31**, 260 (1980) (translation)].
- [6] J. E. Kim, Weak-Interaction Singlet and Strong CP Invariance, *Phys. Rev. Lett.* **43**, 103 (1979).
- [7] M. A. Shifman, A. I. Vainshtein and V. I. Zakharov, Can confinement ensure natural CP invariance of strong interactions?, *Nucl. Phys. B* **166**, 493 (1980).
- [8] K. A. Meissner and H. Nicolai, Effective action, conformal anomaly and the issue of quadratic divergences, *Phys. Lett. B* **660**, 260 (2008); [arXiv:0710.2840 [hep-th]].
- [9] E. Witten, “Some Properties of O(32) Superstrings, *Phys. Lett. B* **149**, 351 (1984).
- [10] P. Svrcek and E. Witten, Axions In String Theory, *JHEP* **06**, 051 (2006).
- [11] O. Lebedev and S. Ramos Sanchez, The NMSSM and String Theory, *Phys. Lett. B* **684**, 48 (2010).
- [12] M. Cicoli, M. Goodsell and A. Ringwald, The type IIB string axiverse and its low-energy phenomenology, *JHEP* **1210**, 146 (2012).
- [13] L. Covi, J. E. Kim and L. Roszkowski, Axinos as Cold Dark Matter, *Phys. Rev. Lett.* **82**, 4180 (1999).
- [14] G. G. Raffelt, Axions: Motivation, limits and searches, *J. Phys. A* **40**, 6607 (2007); [arXiv:hep-ph/0611118].
- [15] L. D. Duffy and K. van Bibber, Axions as Dark Matter Particles, *New J. Phys.* **11**, 105008 (2009).
- [16] P. Sikivie, Dark matter axions, *Int. J. Mod. Phys. A* **25**, 554 (2010).
- [17] H. Baer, A. D. Box and H. Summy, Neutralino versus axion/axino cold dark matter in the 19 parameter SUGRA model, *JHEP* **1010**, 023 (2010).
- [18] T. W. Donnelly, S. J. Freedman, R. S. Lytel, R. D. Peccei, and M. Schwartz, Do Axions Exist?, *Phys. Rev. D* **18**, 1607 (1978).
- [19] A. Zehnder, S. J. Freedman, R. S. Lytel, R. D. Peccei, and M. Schwartz, Axion Search in a Monochromatic Transition: A New Lower Limit for the Axion Mass, *Phys. Lett.* **104B**, 494 (1981).
- [20] I. G. Irastorza, and J. Redondo, New experimental approaches in the search for axion-like particles, *Prog. Part. Nucl. Phys.* **102**, 89 (2018).
- [21] L. Di Luzio, M. Giannotti, E. Nardi, and L. Vasinelli, The landscape of QCD axion models, *Phys. Rep.* **870**, 1 (2020).
- [22] F. Wilczek, Two applications of axion electrodynamics, *Phys. Rev. Lett.* **58**, 1799 (1987).
- [23] R. Li, J. Wang, X. Qi, and S.-C. Zhang, Dynamical Axion Field in Topological Magnetic Insulator, *Nature Phys.* **6**, 284 (2010).
- [24] Y. Gong *et al.*, Experimental Realization of an Intrinsic Magnetic Topological Insulator, *Chin. Phys. Lett.* **36**, 076801 (2019).
- [25] M. M. Otkrov *et al.*, Prediction and observation of an antiferromagnetic topological insulator, *Nature (London)* **576**, 416 (2019).
- [26] C. Liu *et al.*, Robust axion insulator and Chern insulator phases in a two-dimensional antiferromagnetic topological insulator, *Nat. Mater.* **19**, 522 (2020).
- [27] I. I. Klimovskikh *et al.*, Tunable 3D/2D magnetism in the $(\text{MnBi}_2\text{Te}_3)(\text{Bi}_2\text{Te}_3)_m$ topological insulators family, *Quantum Mater.* **5**, 54 (2020).
- [28] H. Ooguri, and M. Oshikawa, Instability in Magnetic Materials with a Dynamical Axion Field, *Phys. Rev. Lett.* **108**, 161803 (2012).
- [29] T. Imaeda, Y. Kawaguchi, Y. Tanaka, and M. Sato, Axion Instability and Nonlinear Electromagnetic Effect, *J. Phys. Soc. Jpn.* **88**, 024402 (2019).
- [30] A. Sekine and K. Nomura, Chiral Magnetic Effect and Anomalous Hall Effect in Antiferromagnetic Insulators with Spin-Orbit Coupling, *Phys. Rev. Lett.* **116**, 096401 (2016).
- [31] K. Taguchi, T. Imaeda, T. Hajiri, T. Shiraishi, and Y. Tanaka, Electromagnetic effects induced by a time-dependent axion field, *Phys. Rev. B* **97**, 214409 (2018).
- [32] A. Sekine, and K. Nomura, Axion electrodynamics in topological materials, *J. Appl. Phys.* **129**, 141101 (2021).
- [33] D. J. E. Marsh, K. C. Fong, E. W. Lentz, L. Šmejkal, and M. N. Ali, Proposal to Detect Dark Matter using Axionic Topological Antiferromagnets, *Phys. Rev. Lett.* **123**, 121601 (2019).
- [34] J. Schütte-Engel, D. J. E. Marsh, A. J. Millar, A. Sekine, F. Chadha-Day, S. Hoof, M. N. Ali, K. C. Fong, E. Hardy, and L. Šmejkal, Axion quasiparticles for axion dark matter detection, *JCAP* **08**, 066 (2021).
- [35] Y. Xiao, H. Wang, D. Wang, R. Lu, X. Yan, H. Guo, C. M. Hu, and K. Xia, Nonlinear level attraction of cavity axion polariton in antiferromagnetic topological insulator, *Phys. Rev. B* **104**, 115147 (2021).

- [36] Z. L. Xiang, S. Ashhab, J. Q. You, and F. Nori, Hybrid quantum circuits: Superconducting circuits interacting with other quantum systems, *Rev. Mod. Phys.* **85**, 623 (2013).
- [37] M. Aspelmeyer, T. J. Kippenberg, and F. Marquardt, Cavity optomechanics, *Rev. Mod. Phys.* **86**, 1391 (2014).
- [38] Y. Xiao, H. Wang, D. Wang, X. Yan, and H. Zhang, Short-wavelength axion dark modes of cavity axion polariton, *Phys. Rev. B* **107**, 085109 (2023).
- [39] R. J. Rivers, *Path integral methods in quantum field theory*, Cambridge Uni. Press, (1987).
- [40] M. Le Bellac, *Thermal field theory*, Cambridge Uni. Press, (1996).
- [41] S. Villalba-Chávez, T. Podszus and C. Müller, Polarization-operator approach to optical signatures of axion-like particles in strong laser pulses, *Phys. Lett. B* **769**, 233 (2017).
- [42] S. Villalba-Chávez, A. E. Shabad and C. Müller, Magnetic dominance of axion electrodynamics: photon capture effect and anisotropy of Coulomb potential, *Eur. Phys. J. C* **81**, 331 (2021).
- [43] J.-M. Zhang, W. Ming, Z. Huang, G.-B. Liu, X. Kou, Y. Fan, K. L. Wang, and Y. Yao, Stability, electronic, and magnetic properties of the magnetically doped topological insulators Bi₂Se₃, Bi₂Te₃, and Sb₂Te₃, *Phys. Rev. B* **88**, 235131 (2013).
- [44] J. Wang, B. Lian, and S.-C. Zhang, Dynamical axion field in a magnetic topological insulator superlattice, *Phys. Rev. B* **93**, 045115 (2016).
- [45] K. Ishiwata, Axion mass in antiferromagnetic insulators, *Phys. Rev. D* **104**, 016004 (2021).
- [46] K. Ishiwata, Topology-insensitive axion mass in magnetic topological insulators, *Phys. Rev. B* **106**, 195157 (2022).
- [47] A. El Kanj, O. Gomonay, I. Boventer, P. Bortolotti, V. Cros, A. Anane, and R. Lebrun, Antiferromagnetic magnon spintronic based on nonreciprocal and nondegenerated ultra-fast spin-waves in the canted antiferromagnet $\alpha - \text{Fe}_2\text{O}_3$, *Sci. Adv.* **9**, adh1601 (2023).
- [48] S. J. Pickart, M. F. Collins, and C.-G. Windsor, Spin-wave dispersion in KMnF₃, *J. Appl. Phys.* **37**, 1054 (1966).
- [49] R. P. Mercier, Thermal radiation in anisotropic media, *Proc. Phys. Soc.* **83**, 811 (1963).
- [50] K. D. Cole, Generalization of Plank's Law of Radiation to Anisotropic Dispersive Media, *Aust. J. Phys.* **30**, 671 (1977).
- [51] We remark that if, on the contrary, the average is taken over the whole ensemble, the mean value of the Cartesian components vanishes, as one could anticipate, due to the equilibrium conditions. Note that no restriction has been imposed on the integration region; there are sectors of the negative momentum domain for which the \mathbf{v} -components are positive.